J. Phys. B: At. Mol. Opt. Phys. **33** (2000) 5329–5341. Printed in the UK PII: S0953-4075(00)15377-5

Charge exchange in slow H^+ + D(1s) collisions

B D Esry†‡‖, H R Sadeghpour†, E Wells‡ and I Ben-Itzhak‡

† Institute for Theoretical Atomic and Molecular Physics, Harvard-Smithsonian Center for Astrophysics, 60 Garden Street, Cambridge, MA 02138, USA

‡ James R Macdonald Laboratory, Department of Physics, Kansas State University, Manhattan, KS 66506, USA

E-mail: esry@phys.ksu.edu

Received 11 July 2000, in final form 29 August 2000

Abstract. We present the elastic and charge exchange cross sections for slow (meV) $H^+ + D(1s)$ collisions based upon a recently formulated adiabatic representation. This representation avoids many of the usual 'translational factor' issues, and those that remain have no significant effect for scattering in the $n = 1$ manifold. The cross sections are converged at the 1% level. The various Feshbach and shape resonances that form in the isotopic gap and in the charge transfer region are identified and compared with previous work. An exact analytical expression for the ratio of $H^+ + D(1s)$ and $D^+ + H(1s)$ charge exchange cross sections suitable for astrophysical simulations is presented.

Collisions between slow protons and atomic hydrogen provide an excellent testing ground for studies of electron transfer because of the simplicity of the system. The transfer of an electron in slow $H^+ + H(1s)$ collisions is a resonant process involving the two lowest electronic states of the transient H_2^+ molecular ion formed during the slow collision. Experiments and theory are in agreement for energies above a few eV (Belyaev 1967, Newman *et al* 1982). As the collision energy is reduced, quantum mechanical effects become important, and experimental difficulties increase. In fact, there have been very few experiments below 10 eV (see the review by Gilbody (1994)).

The $H^+ + D(1s)$ or $D^+ + H(1s)$ collision system is similar electronically to the homonuclear system. In the heteronuclear system, however, electron transfer is only a near-resonant process, again involving the two lowest electronic states of the transient HD^+ molecular ion formed during the slow collision. It is only *near* resonant due to the energy gap of about 3.7 meV between the ground $1s\sigma$ state and the first excited $2p\sigma$ state at the separated-atom limit. Merged beam experiments have produced results down to 0.12 eV (Newman *et al* 1982), still more than 50 meV above the energy range where the calculated results for the various isotopes differ significantly from each other (see figure 1).

Charge transfer in the $H^+ + D(1s)$ system is profoundly more challenging than from the $H^+ + H(1s)$ collision, because of the issues raised by the difference in the nuclear mass, which removes the symmetry present in H_2^+ under the exchange of nuclei. The symmetry-breaking term in HD^+ couples the nuclear and electronic degrees of freedom and produces the splitting of the adiabatic potential energy curves as the nuclei separate. The two lowest adiabatic potential energy curves nearly cross around an internuclear distance of 12 au, inducing non-adiabatic

‖ Author to whom correspondence should be addressed.

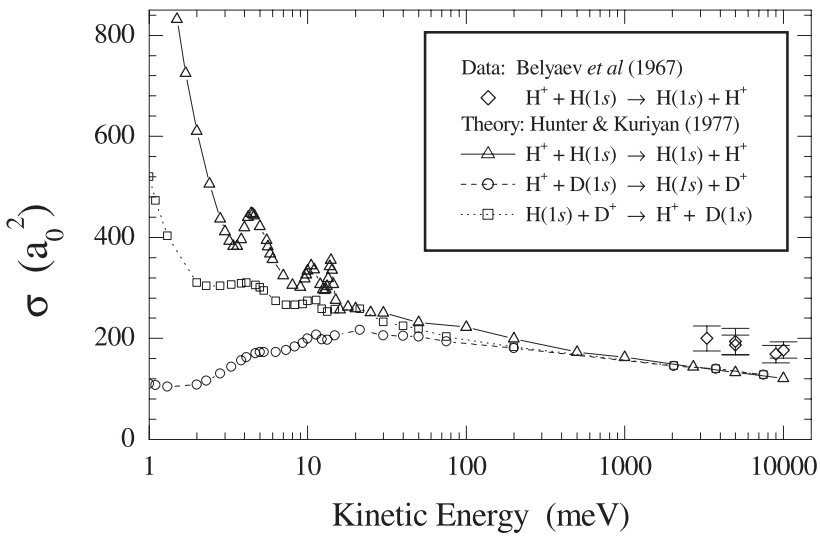

Figure 1. Electron transfer in slow collisions: △, $H^+ + H(1s) \rightarrow H(1s) + H^+$; □, $H^+ + D(1s) \rightarrow H(1s) + D^+$; ○, $H(1s) + D^+ \rightarrow H^+ + D(1s)$. The ◇ are data from Belyaev (1967) while the other symbols are the points calculated by Hunter and Kuriyan (1977b). The energy is the final channel kinetic energy in the centre-of-mass frame.

transitions. At energies larger than about 3.7 meV above the dissociation limit of the 1sσ state, charge transfer can occur via the coupling at this crossing. Because a permanent dipole is formed in the ground and excited electronic states, collisions between H^+ and D can result in radiative vibrational and rotational transitions.

In addition to the fundamental interest, the presence of the deuterium atom in the heteronuclear case makes the collision system important for applications in aeronomy and astrophysics. In planetary atmospheres, charge exchange interactions between abundant isotopic hydrogen neutrals and ions regulate the neutral distribution and escape from the atmosphere. Results of calculations of the differential cross section for electron transfer and elastic scattering in $H^+ + D(1s)$ and $D^+ + H(1s)$ collisions below 10 eV are used to determine temperature-dependent rate coefficients for these processes (Hodges and Breig 1993). In astrophysics, understanding the chemistry of deuterium in the post-recombination era of the early universe is important in evaluating the observed D/H ratio. Using this ratio, it is possible to derive constraints on the primordial deuterium, or, equivalently, on the allowed range of the baryon-to-photon ratio according to the standard big-bang nucleosynthesis (e.g. Burles and Tytler 1998, Penzias *et al* 1977). Additionally, the formation of deuterated molecules (HD, in particular) in the gas phase has an effect on the cooling mechanisms of the primordial gas and on the shocks that led to structure formation, such as galaxies and globular clusters (Palla *et al* 1995). Charge transfer between D and H^+ (or D^+ and H) is one of the first steps in the formation of many deuterated molecules. For example, the primary mechanism for HD formation in interstellar clouds is believed to be the sequence

$$H^+ + D \rightarrow H + D^+ \tag{1}$$

followed by

$$H_2 + D^+ \rightarrow HD + H^+ \tag{2}$$

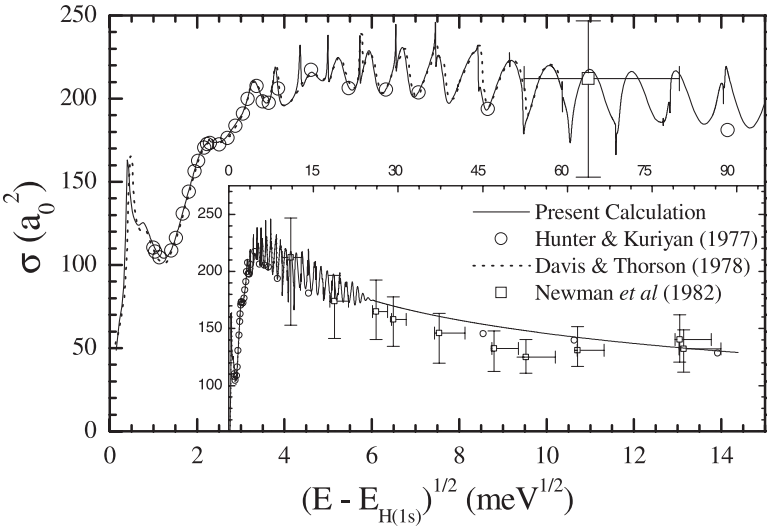

Figure 2. Different electron transfer cross sections in slow H^+ + D(1s) collisions. ○, calculated values of Hunter and Kuriyan (1977b); broken curve, Davis and Thorson (1978); full curve, present work. □, experimental values from Newman *et al* (1982).

(Stancil *et al* 1998, Galli and Palla 1998). Because it is produced in a nearly resonant charge neutralization process, HD plays a role in producing many other deuterated molecules. Rates for all of the many contributing reactions need to be known if the relative abundances of these deuterated molecules are to be determined. Because of the limited number of processes involved in HD formation, the abundance of HD in diffuse interstellar clouds serves as a key diagnostic for models of other molecules with more complicated origins (Watson *et al* 1978).

Two quantum mechanical treatments of the problem of charge transfer in the H^+ + D(1s) system were formulated in the mid-1970s. Hunter and Kuriyan adapted the computational methods developed for the homonuclear system (Hunter and Kuriyan 1975, 1977a) to the heteronuclear system (Hunter and Kuriyan 1977b). The Born–Oppenheimer approximation, which does not discriminate between the two dissociation limits, was employed to separate the nuclear and electronic motions in HD^+ and to reduce the three-body problem to the solution of coupled radial Schrödinger equations for the relative motion of the proton and deuteron. The symmetry-breaking term was introduced in the first order of perturbation theory.

This work was followed by a calculation by Davis and Thorson (1978), where the focus was to search for effects on the elastic and charge-exchange cross sections arising from the nuclear mass asymmetry in HD^+. Their main finding was that the perturbed stationary state (PSS) approach of Hunter and Kuriyan resulted in 'spurious' couplings for the HD^+ system, and therefore had to be removed. The spurious couplings arise because the PSS formulation does not account for the translation of the electron, locally bound to one centre, with respect to the molecular centre of mass (Riera and Salin 1976). Delos and Thorson (1978) suggested essentially that by identifying and ignoring the spurious coupling, a correct theory could be formulated. Their results for the electron transfer cross section are compared with those of Hunter and Kuriyan in figure 2. The lack of structure in Hunter and Kuriyan's (1977b) calculation can be accounted for by differences in the numerical energy mesh. Note, however, that Hunter and Kuriyan's cross sections appear 5–10% lower than those of Davis and Thorson from 30 to 100 meV, due to the accidental overlap of their calculated points with the minima

in the oscillations of the calculated values of Davis and Thorson (1978). The truncated set of two-centre coupled radial wave equations derived by Hunter and Kuriyan was solved more recently using a different numerical technique (Hodges and Breig 1993) and those results did show additional features not seen in the original calculations. They found, for example, a pronounced $J = 10$ shape resonance just slightly above the H(1s) threshold as had Davis and Thorson (1978). The two methods are in reasonable agreement for the overall magnitude of the electron transfer cross section, thus leaving the question of the effect of the 'spurious' couplings unsettled.

We present scattering calculations based upon a recently developed adiabatic representation for diatomic molecular ions (Esry and Sadeghpour 1999). This representation overcomes many of these 'translational factor' deficiencies of the traditional Born–Oppenheimer representation by obtaining the exact finite atomic mass thresholds for the adiabatic potential curves, thereby resulting in the correct asymptotic energies. The departures from the usual Born–Oppenheimer treatment lie in using the centre of mass of the nuclei as the origin of the electronic coordinates and in including selected pieces of the nuclear kinetic energy in the adiabatic Hamiltonian. The resulting adiabatic Hamiltonian in the body frame is

$$H_{\mathrm{ad}} = -\frac{1}{2\mu_{\mathrm{e}}}\nabla_r^2 - \frac{Z_{\mathrm{A}}}{r_{\mathrm{A}}} - \frac{Z_{\mathrm{B}}}{r_{\mathrm{B}}} + \frac{Z_{\mathrm{A}}Z_{\mathrm{B}}}{R} + \frac{J(J+1) - 2\Lambda^2 + \boldsymbol{l}^2}{2\mu_{\mathrm{AB}}R^2} - \frac{(Y+\frac{3}{2})^2}{2\mu_{\mathrm{AB}}R^2}. \tag{3}$$

In this expression, the reduced masses are

$$\frac{1}{\mu_{\mathrm{AB}}} = \frac{1}{m_{\mathrm{A}}} + \frac{1}{m_{\mathrm{B}}}$$
$$\frac{1}{\mu_{\mathrm{e}}} = \frac{1}{m_{\mathrm{A}} + m_{\mathrm{B}}} + 1 \tag{4}$$

while $Z_{\mathrm{A,B}}$ are the charges of nuclei A and B, $r_{\mathrm{A,B}}$ are the distances from the electron to the nuclei and R is the internuclear distance. The quantum numbers J and Λ represent the usual total orbital angular momentum and its projection on the internuclear axis, respectively. The operator Y originates from the radial part of the nuclear kinetic energy and is given in prolate spheroidal coordinates as (Esry and Sadeghpour 1999)

$$Y = \frac{1}{\xi^2 - \eta^2}\left[(\xi + \alpha\eta)\left(\xi^2 - 1\right)\frac{\partial}{\partial\xi} + (\eta + \alpha\xi)\left(1 - \eta^2\right)\frac{\partial}{\partial\eta}\right]$$

where $\alpha = \frac{m_A - m_B}{m_A + m_B}$ is the mass asymmetry parameter and is nearly $\frac{1}{3}$ for HD^+. The operator $\boldsymbol{l}^2$ in equation (3) comes from the angular part of the nuclear kinetic energy and is the usual electronic orbital angular momentum. Given the adiabatic Hamiltonian in equation (3), the electronic wavefunctions and potential energies are found by solving

$$H_{\mathrm{ad}}\Phi_\nu^\Lambda(R;\boldsymbol{r}) = U_\nu^\Lambda(R)\Phi_\nu^\Lambda(R;\boldsymbol{r}) \tag{5}$$

where the total wavefunction Ψ is expanded as

$$\Psi(\boldsymbol{R},\boldsymbol{r}) = \sum_{\nu\Lambda}\frac{1}{R^{5/2}}F_\nu^\Lambda(R)\tilde{D}_{\Lambda M}^{(J)}(\phi,\theta,0)\Phi_\nu^\Lambda(R;\boldsymbol{r}). \tag{6}$$

Finally, the equations satisfied by the radial wavefunctions $F_\nu^\Lambda(R)$ in equation (6) are

$$\left[-\frac{1}{2\mu_{\mathrm{AB}}}\frac{\mathrm{d}^2}{\mathrm{d}R^2} + U_\nu^\Lambda\right]F_\nu^\Lambda - \frac{1}{2\mu_{\mathrm{AB}}}\sum_\lambda\left[2P_{\nu\lambda}^\Lambda\frac{\mathrm{d}}{\mathrm{d}R} + Q_{\nu\lambda}^\Lambda\right]F_\lambda^\Lambda$$
$$-\frac{1}{2\mu_{\mathrm{AB}}R^2}\sum_\lambda\left[\sqrt{J(J+1) - \Lambda(\Lambda+1)}C_{\nu\lambda}^{\Lambda-}F_\lambda^{\Lambda-1}\right.$$
$$\left.+\sqrt{J(J+1) - \Lambda(\Lambda-1)}C_{\nu\lambda}^{\Lambda+}F_\lambda^{\Lambda+1}\right] = EF_\nu^\Lambda. \tag{7}$$

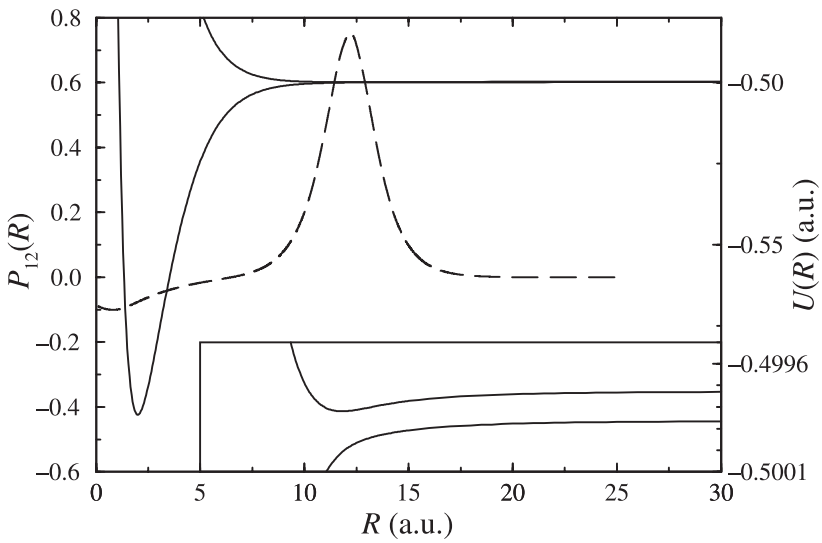

Figure 3. Calculated lowest two adiabatic potential energy curves (full curves) and the P-matrix coupling between them (broken curve). The inset shows an expanded region around the H(1s) and D(1s) thresholds.

The last two terms describe rotation–electronic coupling. The coupling matrices $\boldsymbol{P}$ and $\boldsymbol{Q}$ account for the non-adiabatic effects resulting from the action of the nuclear radial derivatives on the channel functions. Explicitly,

$$P^{\Lambda}_{\nu\lambda} = \left\langle \Phi^{\Lambda}_{\nu} \left| \frac{\partial}{\partial R} - \frac{Y + \frac{3}{2}}{R} \right| \Phi^{\Lambda}_{\lambda} \right\rangle \tag{8}$$

and

$$Q^{\Lambda}_{\nu\lambda} = \left\langle \Phi^{\Lambda}_{\nu} \left| \frac{\partial^2}{\partial R^2} - \frac{2(Y + \frac{3}{2})}{R}\frac{\partial}{\partial R} + \frac{Y + \frac{3}{2}}{R^2} \right| \Phi^{\Lambda}_{\lambda} \right\rangle \tag{9}$$

and the Coriolis coupling matrix elements are

$$C^{\Lambda\pm}_{\nu\lambda} = \langle \Phi^{\Lambda\pm 1}_{\nu} \, |l_{\pm}| \, \Phi^{\Lambda}_{\lambda} \rangle$$

where $l_{\pm}$ are the usual angular momentum raising and lowering operators. In the present study, spectroscopic precision is not warranted, so the Coriolis coupling is neglected.

Figure 3 shows the two lowest adiabatic potential curves for HD^+ and the P-matrix coupling between them. Note that the asymptotic limit of the adiabatic potentials are the exact atomic thresholds $\frac{\mu_D}{2}$ and $\frac{\mu_H}{2}$, respectively, where $\mu_D^{-1} = 1 + \frac{1}{m_D}$ and $\mu_H^{-1} = 1 + \frac{1}{m_H}$. The radial equations were solved using the variational R-matrix method (Greene and Jungen 1984) and expanding the radial solutions on B-splines. The scattering and reaction matrices are obtained using conventional scattering techniques.

To meet the present goal of obtaining cross sections converged to $\sim 1\%$, only the $n = 1$ curves shown in figure 3 were needed. The potential energy curves converging to H($n = 2$) and D($n = 2$) begin to contribute at about the 1% level only for collision energies near 10 eV—near the minimum of the lowest $n = 2$ curve. Over the range of energies approximately 1–8 eV above the H(1s) threshold, partial waves up to $J = 300$ were included to obtain convergence

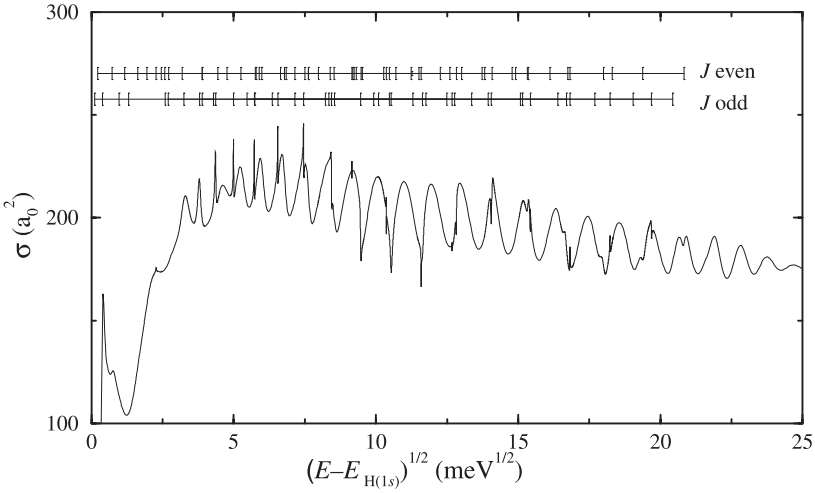

Figure 4. Calculated charge transfer cross sections in slow H^+ + D(1s) collisions as a function of $\sqrt{E - E_{H(1s)}}$. The vertical bars at the top of the figure locate the shape resonances tabulated in table 1.

to 1%, while 70–100 partial waves were included for energies up to 1 eV above the H(1s) threshold. For energies in the gap between the D(1s) and H(1s) thresholds, only 20 partial waves were needed for convergence, in part because the 1sσ centrifugal barrier goes above the H(1s) threshold at $J \approx 10$.

We show in figure 2 the comparison between the present charge exchange cross section and previous calculations. The agreement with the results of Davis and Thorson is reasonable, although their work still lacks the energy resolution needed to resolve many of the resonances we find. We follow their example and attempt to identify each resonance in the charge exchange cross section. Figure 4 shows our calculated charge exchange cross section on a square root energy scale referred to the H(1s) threshold with the position of each resonance marked across the top of the figure (even and odd J values have been indicated separately for clarity). All of the resonances marked in the figure are shape resonances, although some were labelled 'orbiting resonances' by Davis and Thorson. They use this label to distinguish resonances that lie just above the top of the centrifugal barrier from more typical shape resonances below the barrier. These orbiting resonances are quite broad and often overlap a narrower resonance with the same J just below the top of the barrier, and thus were not located for some of the higher Js. The position of each resonance is shown in table 1 along with the vibrational and rotational quantum numbers. The vibrational quantum number is, of course, only a convenient label and refers to the number of nodes within the potential well behind the centrifugal barrier.

The resonance positions were located using the maximum of the time delay

$$\tau = 2\frac{\mathrm{d}\delta}{\mathrm{d}E} \tag{10}$$

where δ is the eigenphase sum. Some of the resonances presented in table 1 lie quite far below the top of the centrifugal barrier and are thus extremely narrow. We did not explicitly locate each of these resonances via equation (10); rather, their position was inferred from a plot of the resonance energies versus J. Analysing the trends in such a plot allowed us to accurately predict the locations of the 'missing' resonances. This approach was verified by an explicit

Table 1. Shape resonances above the H(1s) threshold. Energies marked with an asterisk are estimated resonance positions while the remainder have been explicitly calculated using equation (10). The uncertainty in all resonance positions including those of Moss (1993) is in the last digit shown. The bullets indicate resonances Moss suspected but could not directly calculate.

v	J	E_{vJ} (au)	Moss	v	J	E_{vJ} (au)	Moss
0	42		−0.498 872 763	8	31	−0.498 45*	−0.498 455 013
	43	−0.496 39*	−0.496 395 532		32	−0.497 0481	−0.497 052 310
	44	−0.493 99*	−0.493 999 183		33	−0.495 7838	−0.495 786
	45	−0.491 69*	−0.491 692 826		34	−0.494 7515	
	46	−0.489 48*	−0.489 488 927		35	−0.493 8979	
	47	−0.487 4015	−0.487 407 7	9	29	−0.499 17*	−0.499 175 812
	48	−0.485 4894	•		30	−0.497 8497	−0.497 853 697
	49	−0.483 7777			31	−0.496 6485	−0.496 652
1	40		−0.498 023 146		32	−0.495 6505	•
	41	−0.495 70*	−0.495 702 415		33	−0.494 8599	
	43	−0.493 51*	−0.493 470 721	10	28	−0.498 5173	−0.498 521 155
	44	−0.491 38*	−0.491 342 047		29	−0.497 3896	−0.497 393 05
	45	−0.489 3335	−0.489 339 4		30	−0.496 4362	•
	46	−0.487 5118	•		31	−0.495 6999	
	47	−0.485 9176			32	−0.495 0588	
	48	−0.484 3900		11	26	−0.499 05*	−0.499 056 825
2	39	−0.499 49*	−0.499 490 360		27	−0.498 0082	−0.498 011 53
	40	−0.497 24*	−0.497 246 392		28	−0.497 1127	•
	41	−0.495 08*	−0.495 088 491		29	−0.496 4293	
	42	−0.493 17*	−0.493 031 053		30	−0.495 846	
	43	−0.491 0914	−0.491 097 0	12	24	−0.499 46*	−0.499 464 255
	44	−0.489 3334	•		25	−0.498 5073	−0.498 510 471
	45	−0.487 8233			26	−0.497 6830	•
	46	−0.486 4042			27	−0.497 0569	
3	38	−0.498 63*	−0.498 632 383		28	−0.496 5418	
	39	−0.496 59*	−0.496 549 678	13	23	−0.498 8919	−0.498 894 879
	40	−0.494 65*	−0.494 562 907		24	−0.498 1510	•
	41	−0.492 71*	−0.492 693 78		25	−0.497 5905	
	42	−0.490 9825	−0.490 98		26	−0.497 1446	
	43	−0.489 5298		14	21	−0.499 1699	−0.499 172 600
	44	−0.488 2182			22	−0.498 5233	•
4	37	−0.497 85*	−0.497 856 023		23	−0.498 0379	
	38	−0.495 98*	−0.495 941 781		24	−0.497 6619	
	39	−0.494 21*	−0.494 137 886	15	19	−0.499 3528	−0.499 355 218
	40	−0.492 4773	−0.492 482		20	−0.498 8104	•
	41	−0.491 0625	•		21	−0.498 4087	
	42	−0.489 8434			22	−0.498 1062	
5	35	−0.499 00*	−0.499 007 995	16	17	−0.499 4573	−0.499 453 63
	36	−0.497 17*	−0.497 169 889		18	−0.499 0284	•
	37	−0.495 52*	−0.495 434 038		19	−0.498 7150	
	38	−0.493 8277	−0.493 832 1		20	−0.498 4958	
	39	−0.492 4415	•	17	15	−0.499 5072	−0.499 5089
	40	−0.491 2936			16	−0.499 1977	•
	41	−0.490 1828		18	13	−0.499 5379	•

Table 1. Continued.

v	J	E_{vJ} (au)	Moss	v	J	E_{vJ} (au)	Moss
6	34	−0.498 24*	−0.498 248 166		14	−0.499 3398	
	35	−0.496 63*	−0.495 359 159	19	10	−0.499 6011	•
	36	−0.495 0383	−0.495 042 76		11	−0.499 587	
	37	−0.493 6825	•		12	−0.499 4820	0.499 657 657
	38	−0.492 5846		20	8	−0.499 66	
	39	−0.491 5618			9	−0.499 63	
7	32	−0.499 17*	−0.499 176 819	21	5	−0.499 7087	
	33	−0.497 5870	−0.497 591 574		6	−0.499 6933	
	34	−0.496 1113	−0.496 115 678		7	−0.499 6778	
	35	−0.494 7953	•	22	4	−0.499 7224	
	36	−0.493 7328		23	2	−0.499 7273	
	37	−0.492 8013					

Table 2. Feshbach resonances below the H(1s) threshold. Except for the second column, all energies are below the H(1s) threshold and are reported in cm^{-1}.

	Present			Wolniewicz and Orlikowski		Davis and Thorson		Kennedy *et al*		Lin and Igarashi	
J	E (au)	E	Γ	E	Γ	E	Γ	E	Γ	E	Γ
0	−0.499 754 657	5.886	5.298	5.868	5.261	9.0	9.4	5.840	7.4	5.827	4.26
0	−0.499 728 207	0.0808	0.214	—	—	—	—	0.103	—	—	—
1	−0.499 751 617	5.219	4.668	5.196	4.632	8.44	8.89	4.974	8.8	5.190	3.71
2	−0.499 745 131	3.795	3.369	3.769	3.336	6.58	7.13	3.304	7.1	3.839	2.79
3	−0.499 734 716	1.509	1.725	1.478	1.707	3.51	4.57	0.987	4.6	1.496	1.56

calculation of the time delay in a narrow energy range around two of the predicted locations of missing resonances, for $(v, J) = (10, 28)$ and $(7, 33)$. The remaining resonances predicted using the above scheme are indicated in the table with asterisks.

In table 1 we also show some of the resonance positions calculated by Moss (1993) for comparison. Moss used an artificial channel method and was able to find primarily the low-lying shape resonances. In fact, Moss found two resonances that our approximate scheme above failed to locate for $v = 0$ and 1. All of our estimated positions, however, agree well with those of Moss, generally to four or five digits. Furthermore, where our coupled channel results overlap with those of Moss, the agreement is somewhat better with discrepancies generally occurring in the sixth digit. The bullets in the table indicate resonances that Moss suspected but could not calculate. We should note that the results of Moss account for the Σ–Π Coriolis coupling, while ours do not. For low Js ($J \leqslant 3$), this correction is of the order of 0.001 cm^{-1} (Balint-Kurti *et al* 1990), and increases to roughly 0.01 cm^{-1} already for $J = 5$. For the high values of J in table 1, a similar increase in the magnitude of the shift will bring our results into better agreement with those of Moss.

We note that for J larger than about 10, all shape resonances are primarily 1sσ in character since the 2pσ channel is completely repulsive for all higher J. The main effect of the 2pσ channel in these cases is to contribute a non-resonant background. For low J ($J < 7$), some of the shape resonances are, however, primarily 2pσ in character.

Further quantitative comparison with previous calculations can be made using the Feshbach resonances in the elastic cross section below the H(1s) threshold. This comparison is accomplished in table 2 where the positions of the resonances are again determined from

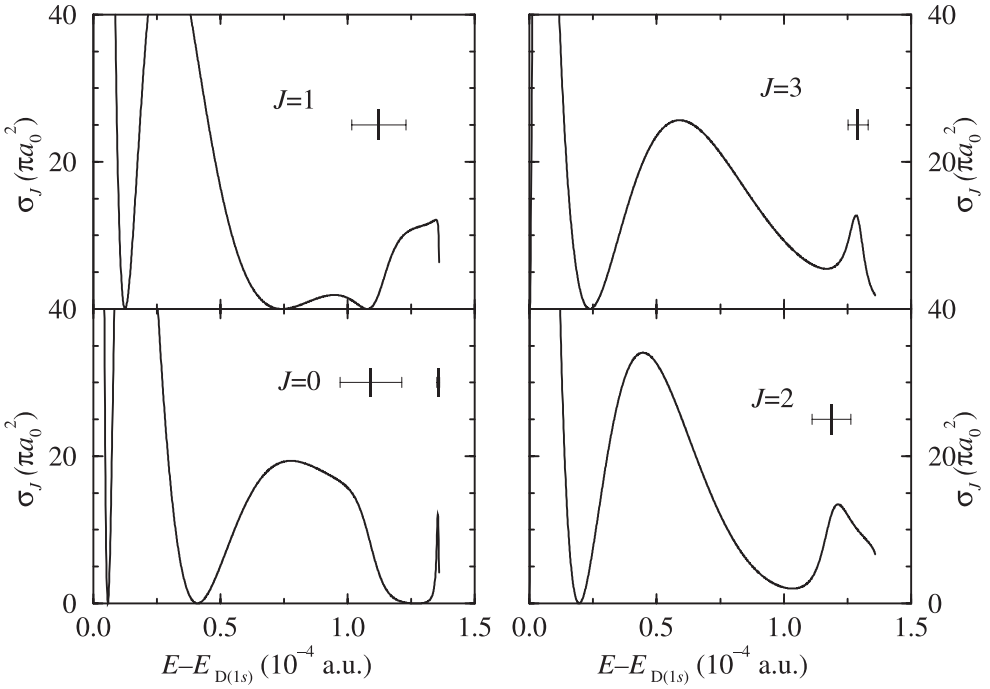

Figure 5. Calculated partial elastic cross sections for $J = 0$–3 between the D(1s) and H(1s) thresholds. The positions and widths of the Feshbach resonances are indicated by vertical bars and horizontal 'error' bars, respectively.

equation (10) and the widths are determined from

$$\Gamma = \frac{4}{\tau_{\max}}. \tag{11}$$

Agreement with Wolniewicz and Orlikowski (1991) to approximately two digits in both the position and width is found. We found a second $J = 0$ resonance whose profile straddles the H(1s) threshold. This resonance had been reported by Kennedy *et al* (1988) leading Wolniewicz and Orlikowski (1991) to specifically attempt to locate it, but they were unable to. The agreement with the results of Davis and Thorson (1978) is much worse even though the total cross sections in figure 2 agree reasonably well. This quantitative difference for the Feshbach resonances could possibly arise from inadequate handling of the spurious couplings by Davis and Thorson. Since the features of the total cross section above a few meV are almost totally controlled by the 1sσ curve, the agreement of the various calculations in figure 2 is not very revealing. The quantitative characteristics of the Feshbach resonances are more stringent tests since they depend critically on the 1sσ–2pσ coupling.

We show in figure 5 the partial elastic cross sections for $J = 0$–3 and mark the location and width of the Feshbach resonances. One striking feature is the large asymmetry for the $J = 0$ and 1 resonances. The higher $J = 0$ resonance and the $J = 2$ and 3 resonances, however, show more recognizable profiles. Just below the H(1s) threshold, the total elastic cross section is dominated by a $J = 10$ shape resonance which overwhelms the second $J = 0$ Feshbach resonance. It turns out that this is the same $J = 10$ shape resonance found by Davis and Thorson (1978) to lie just above the H(1s) threshold. Again, this difference between our calculation and that of Davis and Thorson may be a result of more systematic handling

Table 3. Shape resonances between the D(1s) and the H(1s) thresholds. The uncertainty in all resonance positions including those of Moss (1993) is in the last digit shown.

Present				Moss
J	E (au)	J	E (au)	E (au)
2	−0.499 8630	12	−0.499 8014	−0.499 802 872
3	−0.499 8619	22	−0.499 7458	−0.499 749 086
4	−0.499 8570	27	−0.499 7510	−0.499 755 09
5	−0.499 8445	36	−0.499 8551	−0.499 860 41
6	−0.499 8353			
7	−0.499 8105			
8	−0.499 7604			
9	−0.499 7464			
10	−0.499 7285			

of the 1sσ–2pσ coupling in the present calculation or it may come from the difference built into the potential curves themselves in the present representation. This question could be more definitively answered in a hyperspherical calculation—such as that of Igarashi and Lin (1999)—since the hyperspherical approach is free of translational factors.

We have also located shape resonances in the gap and give their positions in table 3. Note that there is no shape resonance for $J = 1$. This results simply from the fact that the barrier is not sufficiently high to support a resonance. Note that there is a shape resonance for all other values of J up to 10. For $J > 10$, the 1sσ centrifugal barrier peaks above the H(1s) threshold, and a shape resonance occurs in the energy gap for only a few values of J. These resonances are also given in table 3 along with their positions as calculated by Moss (1993). The agreement between the present results and those of Moss is quite good and of the same quality as for table 1.

For completeness, the calculated charge transfer and elastic cross sections as a function of collision energy are shown in figure 6 for both $H^+ + D(1s)$ and $H(1s) + D^+$ collision systems.

In many astrophysical models it is assumed that the reactions

$$H^+ + D(1s) \rightarrow H(1s) + D^+$$

and

$$H(1s) + D^+ \rightarrow H^+ + D(1s)$$

occur with equal probability. If, however, the energy of the collision is below about 0.1 eV ($\approx$ 1000 K), this assumption fails. The ratio of the cross sections for the two reactions has been fitted by Galli and Palla (1998) as $R = e^{-43/T}$, where T is the temperature of the gas (the temperature is associated with the kinetic energy above the H(1s) ground state). This expression approaches unity at high temperature so that the charge transfer proceeds in both directions at the same rate in this limit. Below about 200 K, however, this approximate expression underestimates the calculated ratio R, as can be seen from figure 7. Note that this ratio is smooth in contrast to the structure seen in the cross sections for each individual reaction shown in figure 6. To understand this coarse behaviour and derive a simple analytic form for this ratio, we note that the inelastic cross section is given by

$$\sigma_{12} \propto \frac{1}{k_1^2}|S_{12}|^2 \tag{12}$$

with a similar expression for the second reaction. S_{12} is the transition matrix element. In this expression, 1 labels the channel corresponding to the lower threshold, namely $H^+ + D(1s)$; and

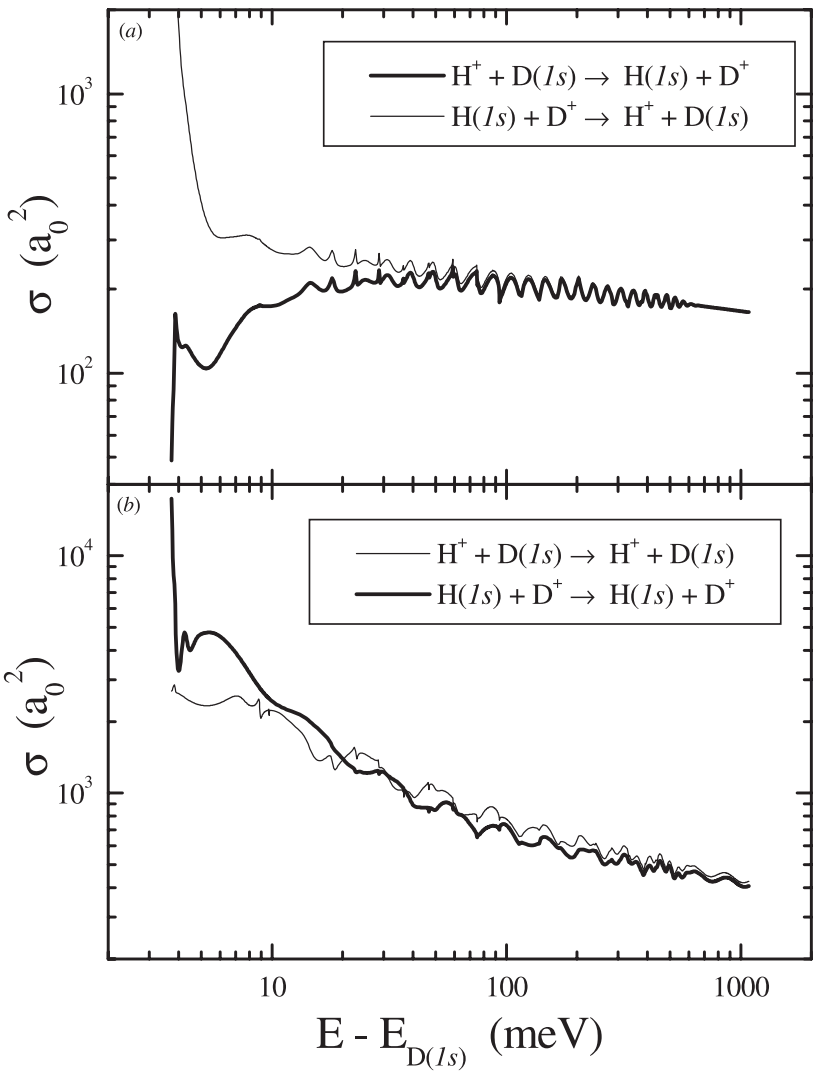

Figure 6. Calculated charge transfer and elastic scattering cross sections in slow H^+ + D(1s) and H(1s) + D^+ collisions.

2, the channel corresponding to the higher threshold, D^+ + H(1s). Thus,

$$R = \frac{\sigma_{12}}{\sigma_{21}} = \frac{(1/k_1^2)|S_{12}|^2}{(1/k_2^2)|S_{21}|^2} = \frac{1/k_1^2}{1/k_2^2} = \frac{E - E_{\mathrm{H(1s)}}}{E - E_{\mathrm{D(1s)}}}. \tag{13}$$

This expression, in contrast with the fit of Galli and Palla (1998), is exact over the entire energy (temperature) range, as long as there are only two channels dominating these reactions. Furthermore, it is as simple to apply as the analytic fit used for astrophysical modelling.

We have presented a calculation of the low-energy charge exchange cross sections for H^++D(1s) using a recently developed adiabatic formulation of the problem that removes many of the translation factor problems of previous calculations. The myriad shape and Feshbach resonances near the $n = 1$ thresholds have been analysed and identified. The ratio of charge

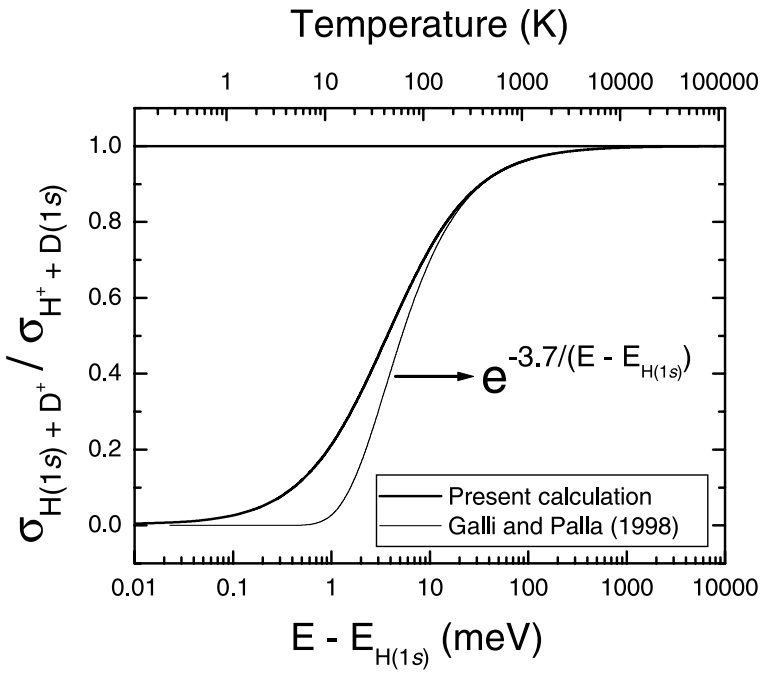

Figure 7. The ratio of the cross section for charge transfer in $H^+ + D(1s)$ to $H(1s) + D^+$ collisions. The full curve is the present theory (see text) and the broken curve is the fit used by Galli and Palla (1998).

exchange cross sections, which has been previously obtained as a fit, is expressed exactly in terms of the collision and the atomic energies.

Acknowledgments

This work was supported in part by a National Science Foundation grant to the Institute for Theoretical Atomic and Molecular Physics at the Harvard-Smithsonian Center for Astrophysics and in part by the Chemical Sciences, Geosciences and Biosciences Division, Office of Basic Energy Sciences, Office of Science, US Department of Energy.

References

Balint-Kurti *et al* 1990 *Phys. Rev.* A **41** 4913
Belyaev V A, Brezhnev B G and Erastov E M 1967 *JETP* **25** 777
Burles S and Tytler D 1998 *Astrophys. J.* **507** 732
Davis J P and Thorson W R 1978 *Can. J. Phys.* **56** 996
Delos J B and Thorson W R 1978 *Phys. Rev.* A **18** 117, 135
Esry B D and Sadeghpour H R 1999 *Phys. Rev.* A **60** 3604
Galli D and Palla F 1998 *Astron. Astrophys.* **335** 403
Gilbody H B 1994 *Adv. At. Mol. Opt. Phys.* **33** 149
Greene C H and Jungen Ch 1984 *Adv. At. Mol. Phys.* **21** 51
Hodges R R Jr and Breig E L 1993 *J. Geo. Res.* **98** 1581
Hunter G and Kuriyan M 1975 *Proc. R. Soc.* A **341** 491
——1977a *Proc. R. Soc.* A **353** 575
——1977b *Proc. R. Soc.* A **358** 321

Igarashi A and Lin C D 1999 *Phys. Rev. Lett.* **83** 4041
Kennedy R A, Moss R E and Sadler I A 1988 *Mol. Phys.* **64** 177
Moss R E 1993 *Mol. Phys.* **78** 371
Newman J H, Cogan J D, Ziegler D L, Nitz D E, Rundel R D, Smith K A and Stebbings R F 1982 *Phys. Rev.* A **25** 2976
Palla F, Galli D and Silk J 1995 *Astrophys. J.* **451** 44
Penzias A A, Wannier P G, Wilson R W and Linke R A 1977 *Astrophys. J.* **211** 108
Riera A and Salin A 1976 *J. Phys. B: At. Mol. Phys.* **9** 2877
Stancil P C, Lepp S and Dalgarno A 1998 *Astrophys. J.* **509** 1
Watson W D, Christensen R B and Deissler R J 1978 *Astron. Astrophys.* **69** 159
Wolniewicz L and Orlikowski T 1991 *Mol. Phys.* **74** 103